

# Commissioning of the TrueBeam STx 6 MV FFF Beam in the RayStation Treatment Planning System for SRS and SBRT Treatments

Yongsook C. Lee\*, Yongbok Kim

Department of Radiation Oncology, The University of Arizona, Tucson, Arizona, USA

Email: \*dr.cecilialee@hotmail.com

**How to cite this paper:** Lee, Y.C. and Kim, Y. (2021) Commissioning of the TrueBeam STx 6 MV FFF Beam in the RayStation Treatment Planning System for SRS and SBRT Treatments. *International Journal of Medical Physics, Clinical Engineering and Radiation Oncology*, 10, 16-37.

<https://doi.org/10.4236/ijmpcero.2021.101003>

**Received:** December 1, 2020

**Accepted:** February 6, 2021

**Published:** February 9, 2021

Copyright © 2021 by author(s) and Scientific Research Publishing Inc. This work is licensed under the Creative Commons Attribution International License (CC BY 4.0).

<http://creativecommons.org/licenses/by/4.0/>



Open Access

## Abstract

**Purpose:** The purpose of this study is to provide technical information on commissioning the TrueBeam STx 6 MV flattening-filter free (FFF) beam in the RayStation treatment planning system (TPS) for stereotactic radiosurgery (SRS) and stereotactic body radiation therapy (SBRT) treatments. **Methods:** For beam modeling, percent depth dose curves, profiles and output factors for jaw-collimated fields and stereotactic cones as well as X-jaws transmission were measured. For multi-leaf collimator (MLC) modeling, MLC model parameters such as offset, gain, curvature, leaf tip width, tongue and groove and transmission were determined and output factors for MLC-collimated fields were measured. Absolute dose calibration was also performed. For beam model and MLC model validation, the American Association of Physicists in Medicine Task Group-119 plans, clinical SRS and SBRT plans and end-to-end testing were performed. **Results:** Beam characteristics of the 6 MV FFF beam agreed well with those in the literature. Validation results showed that our beam model and MLC model were acceptable for SRS and SBRT treatments. **Conclusions:** The technical information and dosimetric data provided in this study will be a useful reference for other clinics/institutions which will commission the same machine energy in the RayStation TPS.

## Keywords

Commissioning, TrueBeam STx, 6 MV Flattening-Filter Free (FFF), RayStation, Stereotactic Radiosurgery (SRS) and Stereotactic Body Radiation Therapy (SBRT)

## 1. Introduction

Major medical linear accelerator (linac) vendors such as Varian (Varian Medical

Systems, Palo Alto, CA) and Elekta (Elekta AB, Stockholm, Sweden) provide flattening filter-free (FFF) photon beam options [1]. Their 6 MV FFF and 10 MV FFF beams allow for dose rates up to 1400 MU/min and 2400 MU/min, respectively [2] [3]. Such high dose rate beams have improved treatment efficiency and accuracy [4]. Stereotactic radiosurgery (SRS) and stereotactic body radiation therapy (SBRT) which are high fractional dose radiotherapy treatments with small fields can predominantly benefit from the FFF beams [4].

Commissioning photon, electron or proton beams in a treatment planning system (TPS) is a tedious and time-consuming task but a very crucial procedure for accurate dose calculations and treatment delivery. Commissioning beams in a TPS is TPS-specific and thus, each TPS requires specific measurement data for beam/MLC modeling and specific setups for beam scans and other measurements. There are several publications on commissioning of linacs with FFF beams [2] [5] [6] and of TPS for photon beams [7] [8] [9]. Chang *et al.* presented nine sets of recommended beam data for the Eclipse (Varian Medical Systems, Palo Alto, CA) TPS, commissioning of intensity modulated radiation therapy (IMRT), volumetric modulated arc therapy (VMAT), image-guided radiation therapy and gating systems,  $P_{ion}$  of FFF beams and small field dosimetric data for three Varian TrueBeam linacs [2]. Glide-Hurst *et al.* reported mechanical and dosimetric data, IMRT commissioning and end-to-end testing results for five TrueBeam linacs from three different institutions [5]. Beyer compared commissioning beam data between two Varian C-series linacs and three TrueBeam linacs [6]. Chen *et al.* and Savini *et al.* presented MLC modeling and validation results in the RayStation (RaySearch Laboratories, Stockholm, Sweden) TPS for Varian C-series linacs [7] [8]. Saez *et al.* developed a novel procedure for optimizing MLC parameters and applied the method to RayStation [9]. However, these studies did not discuss dosimetric data and measurement setups required for commissioning photon beams in RayStation. More importantly, comprehensive steps and dosimetric data for square fields and stereotactic cones for assisting inexperienced physicists with commissioning photon beams in RayStation are not available in a single article format.

The goal of this work, therefore, is to provide detailed technical information on commissioning the TrueBeam STx 6 MV FFF beam in the RayStation TPS. As aforementioned, other linac commissioning tasks are presented in the literature and thus, they are out of scope in this work. Instead, this work details measurement methods, measurement data required by RayStation and beam model/MLC model validation. For SRS and SBRT treatments, dosimetric data for small square fields  $\leq 2 \times 2 \text{ cm}^2$  and Varian stereotactic cones are included in this work. Beam model/MLC model validation was mainly focused on SRS and SBRT plans.

## 2. Methods

### 2.1. Measurements

The RayStation TPS requires specific measurement data for beam modeling and

MLC modeling. Data for beam modeling include beam scans (percent depth dose (PDD) curves and profiles) and output factors for jaw-collimated fields and stereotactic cones, and X-jaws transmission. Data for MLC modeling include MLC model parameters and output factors for MLC-collimated fields. Absolute dose calibration is also required. **Figure 1** shows a summary of measurement data for beam commissioning and detailed description for measurements is in each section below. Measurements (PDDs, profiles and output factors) for beam modeling and absolute dose calibration should be performed at the same source-to-surface distance (SSD). In this work, SSD of 100 cm was chosen and all the measurements listed in **Figure 1** were made at SSD of 100 cm. Measurement data, measurement setups and equipment/detectors for beam commissioning are summarized in **Table 1** and **Table 2**. For equipment/detector selection and measurement setups/techniques, the American Association of Physicists in Medicine Task Group (AAPM TG)-106 guidelines were followed [10]. The RayStation version used in this study was 8A.

**Table 1.** Measurement data, measurement setup and equipment/detectors for commissioning the TrueBeam STx 6MV FFF beam in the RayStation treatment planning system.

Measurement data		Measurement setup		Equipment/detectors
<b>Beam modeling</b>				
Beam scans	PDDs	Square fields (Jaws collimated)*	SSD: 100 cm	3D water tank, ion chamber(s), diode, reference chamber
		Stereotactic cones†	SSD: 100 cm	3D water tank, diode, reference chamber
	Profiles	Square fields (Jaws collimated)*	SSD: 100 cm; depth: $d_{max}$ , 5 cm, 10 cm, 20 cm	3D water tank, ion chamber(s), diode, reference chamber
		Stereotactic cones†	SSD: 100 cm; depth: $d_{max}$ , 5 cm, 10 cm	3D water tank, diode, reference chamber
Output factors	Square fields (Jaws collimated)*		SSD: 100 cm; depth: 10 cm	3D water tank, ion chamber, diode
	Stereotactic cones†		SSD: 100 cm; depth: 10 cm	3D water tank, ion chamber, diode
	X-jaws transmission		SSD: 100 cm; depth: $d_{max}$	3D water tank, farmer-type ion chamber
<b>MLC modeling</b>				
MLC model parameters	x-position offset, gain and curvature; y-position gain	PDDs	SSD: 100 cm	3D water tank, ion chamber(s), diode, reference chamber
		Profiles	SSD: 100 cm; depth: $d_{max}$ , 5 cm, 10 cm, 20 cm	
	Leaf tip width	Custom plan	SSD: 100 cm; depth: 10 cm	3D water tank, diode, reference chamber
	Tongue and groove	Custom plan	SSD: 100 cm; depth: 10 cm	3D water tank, diode, reference chamber
	Transmission	Custom plan	SSD: 100 cm; depth: $d_{max}$	3D water tank, farmer-type ion chamber
Output factors	Square fields (MLC collimated)‡		SSD: 100 cm; depth: 10 cm	3D water tank, ion chamber, diode
<b>Absolute dose calibration</b>				
AAPM TG 51		SSD: 100 cm; depth: 10 cm; Field size: $10 \times 10 \text{ cm}^2$		1D water tank, farmer-type ion chamber

\*(per side in cm) 0.6, 1, 2, 3, 4, 5, 6, 8, 10, 15, 20, 30, 40; †(diameter in mm) 4, 5, 7.5, 10, 12.5, 15, 17.5; ‡(per side in cm) 1, 2, 3, 4, 5, 6, 8, 10, 12, 15, 20.

**Table 2.** Equipment/detectors and their models used for measurements.

Equipment/detector	Model	Purpose
3D water tank	Sun Nuclear 3D SCANNER™	All measurements except for absolute dose calibration
1D water tank	Sun Nuclear 1D SCANNER™	Absolute dose calibration
Ion chamber	Sun Nuclear SNC125c™ (volume: 0.125 cm³)	Beam scans and output factors for square fields $\geq 4 \times 4$ cm²
Diode	Sun Nuclear Edge Detector™ (volume: 0.0019 cm³)	Beam scans for square fields $\leq 3 \times 3$ cm² and stereotactic cones; Output factors for square fields $\leq 4 \times 4$ cm² and stereotactic cones
Reference chamber	Sun Nuclear Reference Detector (parallel plate chamber, volume: 39 cm³)	Beam scans for square fields $\leq 3 \times 3$ cm² and stereotactic cones
Farmer-type ion chamber	Standard Imaging Exradin A12 (volume: 0.64 cm³)	Absolute dose calibration, MLC transmission and X-jaws transmission
	Sun Nuclear MapCHECK™ 2	MPPG 5.a. Tests including AAPM TG-119 plans
QA device	Sun Nuclear SRS MapCHECK™ and StereoPHAN™	Clinical SRS and SBRT plans
	Sun Nuclear StereoPHAN™ and Standard Imaging Exradin A16 (volume: 0.007 cm³)	End-to-End testing

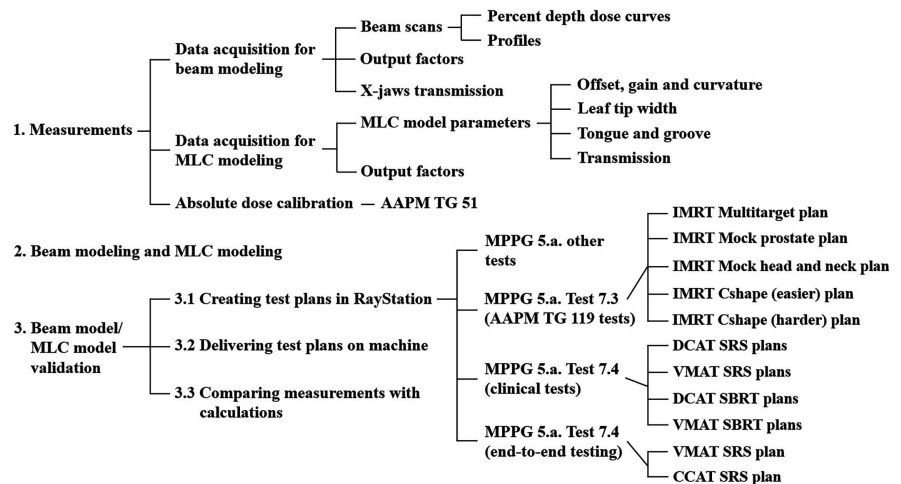


**Figure 1.** An overview of procedures for beam commissioning in the RayStation treatment planning system. Abbreviations) MLC: multi-leaf collimator; AAPM TG: American Association of Physicists in Medicine Task Group; MPPG: medical physics practice guideline; IMRT: intensity modulated radiation therapy; DCAT: dynamic conformal arc therapy; VMAT: volumetric modulated arc therapy; CCAT: circular collimator arc therapy.

***Beam scans for jaw-collimated square fields and stereotactic cones***

PDDs and profiles (cross-plane and in-plane) for jaw-collimated square fields and Varian stereotactic cones were acquired. For beam scans, a three-dimensional (3D) cylindrical water tank, an ion chamber or a diode detector and a reference chamber were used. The 3D water tank (3D SCANNER™, Sun Nuclear Corporation, Melbourne, FL) and its software (Sun Nuclear SNC Dosimetry™) used in this study allowed for an auto-setup which minimizes inter- and intra-user setup variations [11]. For square fields, field sizes ranged from  $0.6 \times 0.6$  cm² to  $40 \times 40$  cm² and were determined by the jaw settings with MLCs parked (*i.e.*, jaw only

collimated) (**Table 1**). For stereotactic cones, cone diameters ranged from 4 mm to 17.5 mm (**Table 1**). For square fields  $\geq 4 \times 4 \text{ cm}^2$ , two identical ion chambers (Sun Nuclear SNC125c<sup>TM</sup>) were used for field and reference detectors. For square fields  $\leq 3 \times 3 \text{ cm}^2$  and stereotactic cones, a diode detector (Sun Nuclear Edge Detector<sup>TM</sup>) and a reference chamber (Sun Nuclear Reference Detector) were used. Profiles for square fields were taken at four different depths ( $d_{\text{max}}$ , 5 cm, 10 cm and 20 cm), whereas those for stereotactic cones were taken at three depths ( $d_{\text{max}}$ , 5 cm and 10 cm) because cones are used for cranial treatments and beam data for 20 cm are not necessary. Effective points of measurement were considered for both ion chamber and diode detector.

After beam scans, beam characteristics of the 6 MV FFF beam were determined. PDD data at depths of 5 cm, 10 cm and 20 cm were taken for square fields and cones. From profiles for square fields and cones, lateral distances between 20% and 80% isodose curves at a depth of 10 cm were taken. An average value of two (left and right) lateral distances from each profile was calculated. This is conventionally defined as penumbra but this definition cannot be applied to FFF beams [5]. For FFF beams, a new penumbra concept called a normalization technique was introduced by Pönisch *et al.* [12]. In this work, for simplicity, the original definition (*i.e.*, lateral distance between 20% and 80% isodose curves) was used as a profile parameter but it was not considered as penumbra for this beam.

#### ***Output factors (OFs) for jaw-collimated square fields and stereotactic cones***

OFs for jaw-collimated square fields and stereotactic cones were measured at a depth of 10 cm in the 3D water tank. First, charges for square fields  $\geq 4 \times 4 \text{ cm}^2$  were collected using an ion chamber (Sun Nuclear SNC125c<sup>TM</sup>). Second, charges for square fields  $\leq 4 \times 4 \text{ cm}^2$  and stereotactic cones were collected using a diode detector (Sun Nuclear Edge Detector<sup>TM</sup>). Then output factors for square fields  $\geq 5 \times 5 \text{ cm}^2$  were calculated using Equation (1). A field size of  $10 \times 10 \text{ cm}^2$  was selected as a reference field.

$$\text{OF} = \frac{M_{\text{IC}}(\text{Square Field})}{M_{\text{IC}}(\text{Reference Field})} \quad (1)$$

where  $M_{\text{IC}}(\text{Square Field})$  and  $M_{\text{IC}}(\text{Reference Field})$  are uncorrected ion chamber (IC) readings for a square field of interest and for the reference field of  $10 \times 10 \text{ cm}^2$ , respectively. For square fields  $\leq 4 \times 4 \text{ cm}^2$  and stereotactic cones, output factors were calculated using Equation (2) (intermediate field method or daisy-chain method) [13]. The daisy-chain method mitigates energy dependent response of the diode detector with changing field size [13]. A field size of  $4 \times 4 \text{ cm}^2$  was selected as an intermediate field.

$$\text{OF} = \frac{M_{\text{diode}}(\text{Square Field or Cone})}{M_{\text{diode}}(\text{Intermediate Field})} \times \frac{M_{\text{IC}}(\text{Intermediate Field})}{M_{\text{IC}}(\text{Reference Field})} \quad (2)$$

where  $M_{\text{diode}}(\text{Square Field or Cone})$  and  $M_{\text{diode}}(\text{Intermediate Field})$  are diode readings for a square field or a cone of interest and for the intermediate field of  $4 \times 4 \text{ cm}^2$ .

$\times 4 \text{ cm}^2$ , respectively, and  $M_{IC}$  (Intermediate Field) and  $M_{IC}$  (Reference Field) are uncorrected ion chamber (IC) readings for the intermediate field of  $4 \times 4 \text{ cm}^2$  and the reference field of  $10 \times 10 \text{ cm}^2$ , respectively.

For square fields  $\leq 2 \times 2 \text{ cm}^2$  and stereotactic cones, field output correction factors ( $k_{Q_{clin}, Q_{msr}}^{f_{clin}, f_{msr}}$ ) were multiplied by measured OFs. Field output correction factors for the diode detector used in this study are required to take into account its over-response in small fields  $\leq 2 \times 2 \text{ cm}^2$  [13] [14]. Correction factors for our measurements were taken from Tanny *et al.*'s study because they used the same measurement setup (depth of 10 cm and SSD of 100 cm) and the same detector (Sun Nuclear Edge Detector<sup>TM</sup>) to obtain the correction factors for the 6 MV FFF beam [14]. For stereotactic cones, cone diameters were converted to equivalent square fields using the relationship of  $S = r\sqrt{\pi}$  where  $S$  is a side of an equivalent square field and  $r$  is a radius of a corresponding cone, and the correction factors from Tanny *et al.* were linearly interpolated [14].

#### ***X-jaws transmission***

X-jaws transmission was determined. X1-jaw and X2-jaw cannot be completely closed and 0.5 cm is the minimum spacing between X1-jaw and X2-jaw. Also, the maximum travel distance of each jaw to the opposite direction is 2 cm. To minimize a dosimetric effect from the 0.5 cm opening, the distance between chamber position and 0.5 cm opening was maximized. As a result, a field size of  $18 \times 40 \text{ cm}^2$  was chosen for open fields. For an X1-jaw closed field, jaws were set to  $(X1, X2, Y1, Y2) = (-2, 2.5, 20, 20)$  with MLCs parked. A Farmer-type ion chamber (Exradin A12, Standard Imaging, Middleton, WI) was placed at  $(x, y, z) = (-11, 0, d_{max})$  in the 3D water tank and charges ( $Rdg X1_{closed}$ ) were collected. For an X1-jaw open field of  $18 \times 40 \text{ cm}^2$ , jaws were set to  $(X1, X2, Y1, Y2) = (20, -2, 20, 20)$  and charges ( $Rdg X1_{open}$ ) were collected at the same chamber location. Measurements ( $Rdg X2_{closed}$  and  $Rdg X2_{open}$ ) were repeated for the X2-jaw. Then ratios of  $Rdg X1_{closed}$  to  $Rdg X1_{open}$  and  $Rdg X2_{closed}$  to  $Rdg X2_{open}$  were taken and an average value of the two ratios was calculated as X-jaws transmission. After beam scans, OF and X-jaws transmission measurements, beam modeling was performed. Details on beam modeling are out of scope in this work.

#### ***MLC model parameters***

The TrueBeam STx linac features a high definition (HD120<sup>TM</sup>) MLC with 2.5 mm central leaves (8 cm) and 5 mm outer leaves (7 cm on either side) projected at isocenter, allowing for a maximum MLC-defined field size of  $40 \times 22 \text{ cm}^2$ . MLC modeling in RayStation requires four MLC model parameters (Figure 1 and Table 1). They include 1) offset, gain and curvature, 2) leaf tip width, 3) tongue and groove and 4) MLC transmission [7] [8] and were measured as follows.

Optimal values for x-position offset, gain and curvature, and y-position gain were determined from cross-plane (x-direction) and in-plane (y-direction) profiles for MLC-collimated square fields. MLC-collimated square fields ranging from  $1 \times 1 \text{ cm}^2$  to  $20 \times 20 \text{ cm}^2$  were created in RayStation (Figure 2 and Table 1). No MLC leaf tip offset was set in x-direction (*i.e.*, closed MLC leaves are at 0

cm) (Figure 2). Jaws were retracted by 0.5 cm from MLCs in each direction. Then PDDs and profiles for the MLC-collimated fields were acquired in the 3D water tank in the same way as beam scans for jaw-collimated fields. Optimal values for offset (cm), gain ( $\text{cm}^{-1}$ ) and curvature ( $\text{cm}^{-2}$ ) were determined such that measured profiles matched well calculated profiles in RayStation.

Optimal values for leaf tip width and tongue and groove width were determined by adopting custom plans created by Savini *et al.* [8]. Two fields in Figure 3 were created in RayStation. Jaws were set to  $40 \times 5 \text{ cm}^2$ . Cross-plane profiles for the fields were taken at a depth of 10 cm in the 3D water tank using a diode detector (Sun Nuclear SNC125c<sup>TM</sup>). After the scans, two profiles were merged into one profile. The optimal value for leaf tip width (cm) was determined such that the measured merged profile matched well the profile calculated in RayStation. In the same fashion, two fields in Figure 4 were created with jaw settings of  $15 \times 22 \text{ cm}^2$ . In-plane profiles for the fields were taken and merged. The optimal value for tongue and groove width (cm) was determined such that the measured merged profile matched well the profile calculated in RayStation.

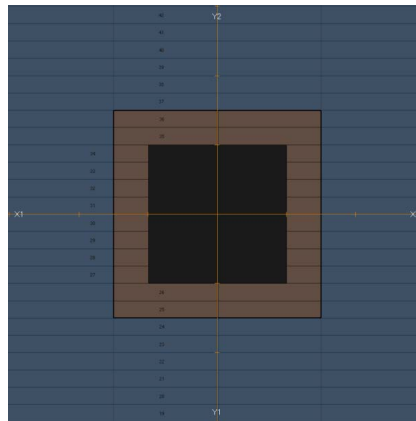


**Figure 2.** A MLC-collimated field ( $2 \times 2 \text{ cm}^2$ ) to determine optimal values for x-position offset, gain and curvature and y-position gain.

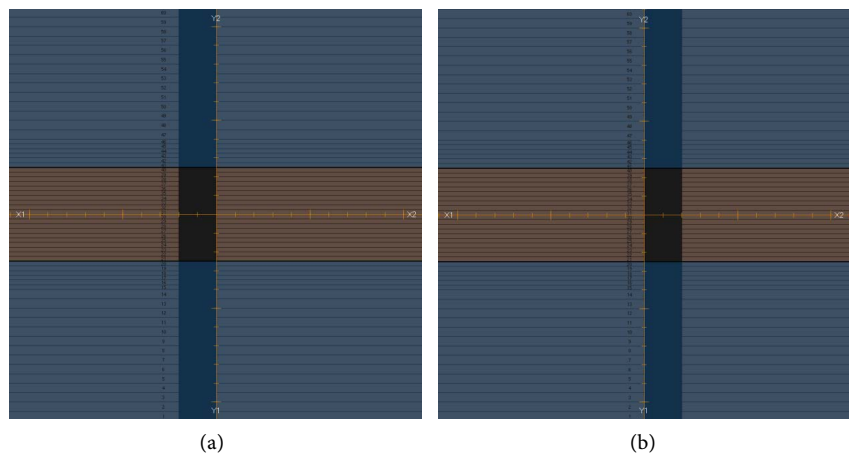


**Figure 3.** (a), (b) Two custom fields to determine the optimal value for leaf tip width. Cross-plane profiles were taken for both fields.

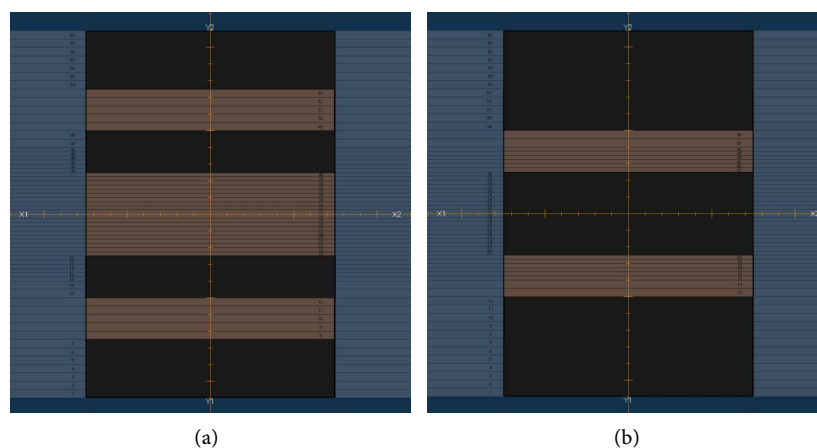


**Figure 4.** (a), (b) Two custom fields to determine the optimal value for tongue and groove width. In-plane profiles were taken for both fields.

MLC transmission was determined by adopting another custom plan created by Savini *et al.* [8]. A field with the MLC bank A completely closed (**Figure 5(a)**) and a corresponding open field (**Figure 5(b)**) were created in RayStation. Jaws were set to  $(X1, X2, Y1, Y2) = (0, 10, 11, 11)$ . A Farmer-type ion chamber (Exradin A12) was placed at  $(x, y, z) = (5, 0, d_{max})$  in the 3D water tank and charges (Rdg  $A_{closed}$  and Rdg  $A_{open}$ ) were collected for the MLC bank A closed and open fields. Field creation in RayStation (**Figure 5(c)** and **Figure 5(d)**) and measurements (Rdg  $B_{closed}$  and Rdg  $B_{open}$ ) were repeated for the MLC bank B. Then ratios of Rdg  $A_{closed}$  to Rdg  $A_{open}$  and Rdg  $B_{closed}$  to Rdg  $B_{open}$  were taken and an average value of the two ratios was calculated as MLC transmission. A Farmer-type ion chamber was used to take into account both inter-leaf transmission and intra-leaf transmission.

#### ***OFs for MLC-collimated square fields***

Following the Medical Physics Practice Guideline (MPPG) 5.a. recommendation (Test 7.2) [15], OFs for MLC-collimated square fields ranging from  $1 \times 1$  cm<sup>2</sup> to  $20 \times 20$  cm<sup>2</sup> were measured (**Table 1**) and compared with OFs calculated in RayStation. In the same way as OFs for jaw-collimated fields, charges were collected at a depth of 10 cm in the 3D water tank and OFs were calculated using Equations (1) and (2). For field sizes  $\leq 2 \times 2$  cm<sup>2</sup>, the field output correction factors taken from Tanny *et al.* were multiplied [14]. In RayStation, dose at the center of the MLC-collimated fields was calculated in a virtual water phantom. A ratio of dose for each field size to that for a field size of  $10 \times 10$  cm<sup>2</sup> was taken as a calculated OF. Then ratios of measured OFs to calculated OFs were taken for comparison.

#### ***Absolute dose calibration***

Dose output of the 6 MV FFF beam was calibrated using the AAPM TG-51 protocol [16], addendum to the TG-51 protocol [17] and Technical Reports Series (TRS) No. 483 [13]. A measurement setup was SSD of 100 cm, a depth of 10 cm and a field size of  $10 \times 10$  cm<sup>2</sup> (**Table 1**). A 1D tank (Sun Nuclear 1D

SCANNER™) and a Farmer-type ion chamber (Exradin A12) were used. The recommendations for FFF beams in the addendum [17] and TRS No. 483 [13] were implemented in this work as follows. For FFF beams, the contribution of scattered photons in the center of the field depends on field size and the energy [13]. As a result, the equivalent uniform square field size ( $S$ ) is not the same as the actual field size [13]. In this study, therefore, for the conventional reference field of  $10 \times 10 \text{ cm}^2$ , %dd(10, 10) was determined from equation (29) in the TRS No. 483 [13]. The equation (29) is

$$\%dd(10,10) = \left[ \%dd(10,S) + 80c(10-S) \right] / \left[ 1 + c(10-S) \right]$$

where  $S = 9.5 \text{ cm}$  for the 6 MV FFF beam and  $c = (54.4 \pm 1.1) \times 10^{-3}$ . %dd(10,  $S$ ) was measured for an actual field size of  $10 \times 10 \text{ cm}^2$  with a 1-mm lead foil in the 1D water tank and considered as %dd(10)<sub>x</sub> in the AAPM TG-51 protocol. After %dd(10, 10) was determined using the equation (29), the  $k_Q$  factor for the A12 chamber was calculated from Equation (1) in the addendum [17]. The Equation (1) is

$$k_Q = A + B \cdot 10^{-3} \cdot \%dd(10)_x + C \cdot 10^{-5} \cdot (\%dd(10)_x)^2$$

where  $A = 1.0146$ ,  $B = 0.777$  and  $C = -1.666$  for the A12 chamber. In this equation, calculated %dd(10, 10) was used as %dd(10)<sub>x</sub>. After dose output was calibrated to 1 cGy/MU at  $d_{\text{max}}$ , absolute dose (cGy/MU) for a depth of 10 cm was determined from %dd(10).

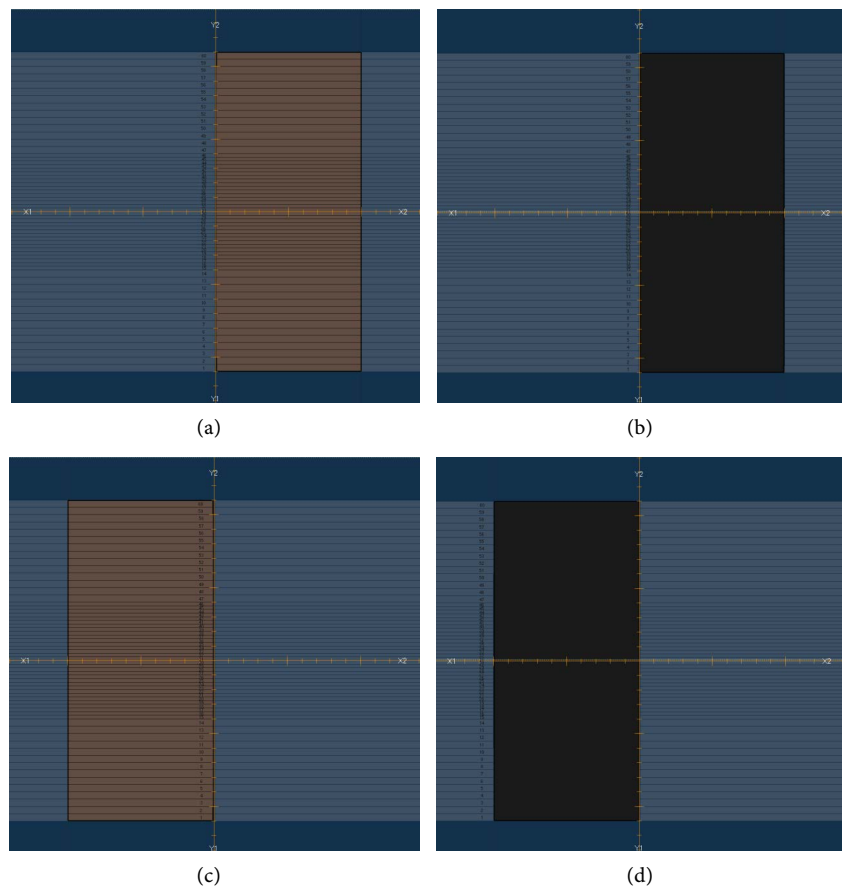


**Figure 5.** MLC (a) closed and (b) open fields for the MLC bank A and MLC (c) closed and (d) open fields for the MLC bank B to determine MLC transmission.

## 2.2. Beam Model/MLC Model Validation Tests

Our beam and MLC models were validated based on the guidelines of MPPG 5.a. [15] and AAPM TG 119 [18]. Tests in Tables 3-7 of MPPG 5.a. were comprehensively performed for the 6 MV FFF beam. Of those, 1) AAPM TG-119 tests (Test 7.3), 2) clinical tests (Test 7.4) and 3) external review (Test 7.5, complete end-to-end test) will be described and presented in this work. **Figure 1** shows a summary of beam model/MLC model validation tests and details for each test are described below. **Table 2** includes the quality assurance (QA) devices used for beam model/MLC model validation.

AAPM TG-119 tests (Test 7.3 from MPPG 5.a.) were performed. In RayStation, five plans (Multitarget, Mock prostate, Mock head/neck, CShape (easier) and CShape (harder)) were created using static IMRT (dynamic MLCs). Following the AAPM TG-119 guidelines, seven or nine beams were configured and plans were optimized to meet dose constraints. Patient-specific QA plans were generated on a solid water phantom with a dose grid size of 2 mm × 2 mm and were delivered using a 2D diode array (Sun Nuclear MapCHECK<sup>®</sup> 2). A depth of dose calculation and delivery was 5 cm in a source-to-axis distance (SAD) setup. Gamma analysis for gamma criteria of 3%/3 mm and 2%/2 mm was performed to compare between measurements and calculations in Sun Nuclear SNC Patient software (version 6.7.4). Absolute dose mode, global normalization and a threshold of 10% were used as in the AAPM TG-119 report.

Clinical tests (Test 7.4 from MPPG 5.a.) were performed. Our institution uses primarily arc (dynamic conformal arc therapy (DCAT) or VMAT) plans for SRS and SBRT treatments. Thus, ten clinical SRS (five DCAT and five VMAT) plans and ten clinical SBRT (five DCAT and five VMAT) plans with a single lesion were selected and re-calculated using the 6 MV FFF beam. The SRS plans had five to seven non-coplanar beams with a prescribed dose ranging from 15 Gy to 24 Gy. The SBRT plans had two coplanar beams with a prescribed dose ranging from 10 Gy to 12 Gy per fraction. Patient-specific QA plans were generated on another 2D diode array with a higher spatial resolution (Sun Nuclear SRS MapCHECK<sup>®</sup>) residing in the Sun Nuclear StereoPHAN<sup>™</sup> with a dose grid size of 1 mm × 1 mm and were delivered using the SRS MapCHECK. A depth of dose calculation and delivery was in the level where diodes are located in a SAD setup. Gamma analysis for gamma criteria of 2%/1 mm and 1%/1 mm was performed to compare between measurements and calculations in Sun Nuclear SRS MapCheck software (version 8.3.0). Absolute dose mode, global normalization and a threshold of 10% were used.

End-to-end testing (Test 7.5 from MPPG 5.a.) was performed. Computed tomography (CT) images of the StereoPHAN<sup>™</sup> with an ion chamber (Standard Imaging Exradin A16) and ion chamber inserts were acquired with a 1.25 mm slice thickness. The CT images were imported in RayStation and two SRS plans were generated based on our institutional clinical practice: one plan using VMAT (five non-coplanar beams) and the other plan using circular collimator

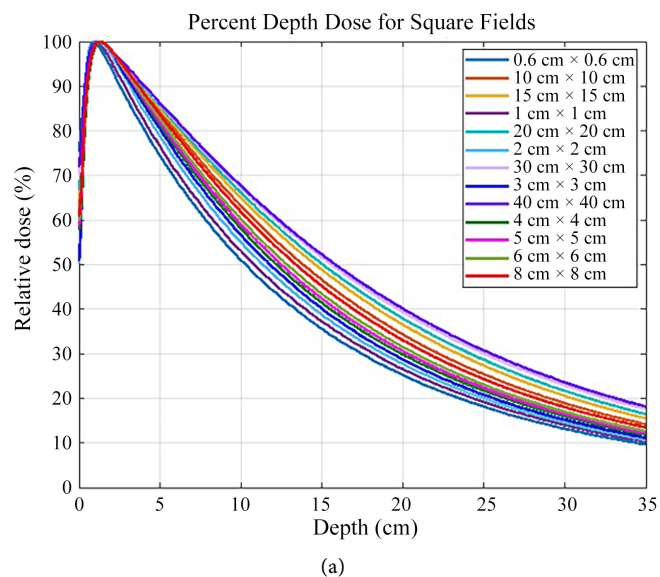
arc therapy (CCAT) with a 17.5 mm cone (six non-coplanar beams). In these plans, the ion chamber was contoured and an isocenter was set to the centroid of the contour. A dose of 21 Gy was prescribed in both plans. As recommended in the Sun Nuclear SRS MapCHECK™ user guide, the StereoPHAN™ was contoured and overridden with a density of 1.2 g/cm<sup>3</sup>. The plans were transferred to a record and verify system (Mosaiq®, Elekta AB, Stockholm, Sweden). Before plan delivery, the Winston-Lutz test was performed to check if isocenter stability was within our institutional tolerance (0.75 mm). A setup of the StereoPHAN™ was verified on six degrees of freedom couch using cone beam CT and the VMAT plan was delivered. Delivered dose to the isocenter was compared with mean dose of the contoured ion chamber in the plan. End-to-end testing was repeated for the cone plan. Before end-to-end testing, the A16 ion chamber was cross-calibrated against an Accredited Dosimetry Calibration Laboratory-calibrated ion chamber (*i.e.*, Exradin A12 ion chamber).

### 3. Results and Discussion

#### 3.1. Measurements

##### *Beam scans and OFs for jaw-collimated square fields and stereotactic cones, and X-jaws transmission*

PDDs and cross-plane profiles for jaw-collimated fields and stereotactic cones are shown in **Figure 6** and **Figure 7**, respectively. **Table 3** presents PDD parameters (PDD (%) at 5 cm, 10 cm and 20 cm) and profile parameter (lateral distance (mm) between 20% and 80% isodose curves at a depth of 10 cm) for each field and each cone. For this energy,  $d_{\max}$  was found to be 1.36 cm. As expected, for the same depth, PDD decreases as field size or cone diameter decreases (**Figure 6**). Also, the lateral distance between 20% and 80% isodose curves decreases with decreasing field size or cone diameter (**Figure 7**). Measured X-jaws transmission was 0.36%.



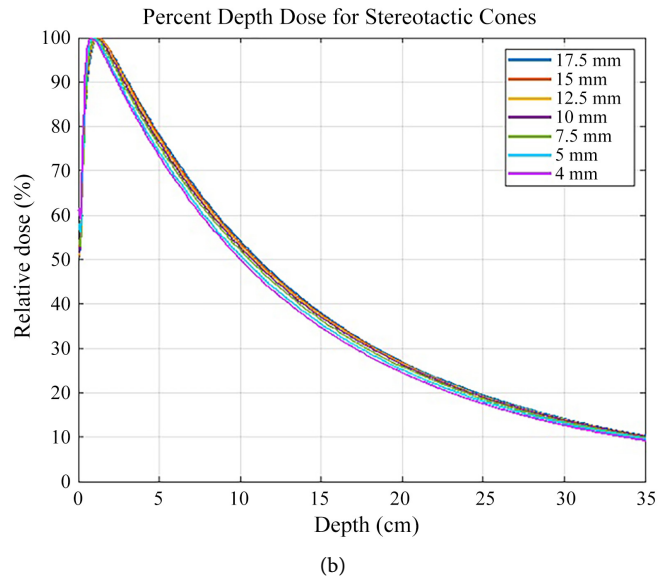


**Figure 6.** PDDs for (a) jaw-collimated square fields and (b) stereotactic cones.

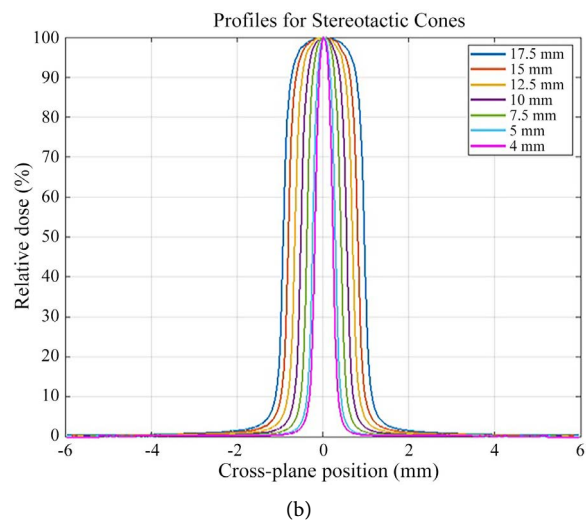
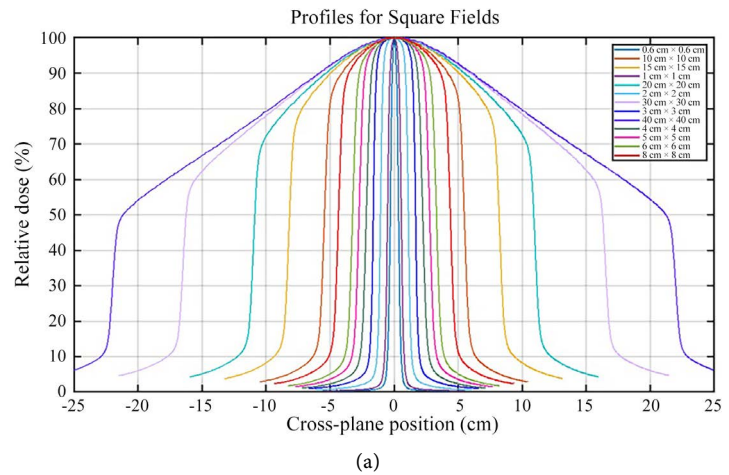


**Figure 7.** Cross-plane profiles at a depth of 10 cm for (a) jaw-collimated square fields and (b) stereotactic cones.

**Table 3.** Percent depth dose and profile parameters for jaw-collimated square fields and stereotactic cones.

Field size (cm <sup>2</sup> )	Percent depth dose (%)						
	5 cm	10 cm	20 cm	Cone diameter (mm)	5 cm	10 cm	20 cm
0.6 × 0.6	74.4	50.9	25.2	4	73.2	50.1	24.6
1 × 1	76.6	53.1	26.6	5	74.1	50.9	25.3
2 × 2	78.8	55.0	27.8	7.5	75.5	52.1	25.9
3 × 3	80.5	56.6	28.7	10	76.4	52.6	26.4
4 × 4	81.3	58.0	29.8	12.5	77.1	53.1	26.7
5 × 5	81.9	59.1	30.6	15	77.5	53.7	26.9
6 × 6	82.8	60.1	31.5	17.5	78.1	54.1	27.0
8 × 8	83.7	61.8	33.1				
10 × 10	84.4	63.2	34.4				
15 × 15	85.1	65.0	36.5				
20 × 20	85.7	66.1	37.9				
30 × 30	86.0	67.1	39.4				
40 × 40	86.2	67.7	40.2				

Lateral distance (mm) between 20% and 80% isodose curves at a depth of 10 cm*					
Field size (cm <sup>2</sup> )	Cross-plane	In-plane	Cone diameter (mm)	Cross-plane	In-plane
0.6 × 0.6	2.3	2.8	4	1.36	1.34
1 × 1	2.6	3.1	5	1.43	1.45
2 × 2	2.8	3.4	7.5	1.59	1.56
3 × 3	3.0/4.9†	3.6/5.3†	10	1.70	1.68
4 × 4	5.1	5.6	12.5	1.78	1.77
5 × 5	5.4	5.9	15	1.84	1.80
6 × 6	5.7	6.2	17.5	1.88	1.84
8 × 8	6.3	6.8			
10 × 10	7.3	7.8			
15 × 15	13.4	14.0			
20 × 20	29.3	29.7			
30 × 30	73.8	74.0			
40 × 40	124.2	124.5			

\*Note that this is not the penumbra definition for FFF beams. †Values were taken from profiles measured using an ion chamber.

Our beam data for jaw-collimated square fields had good agreement with Varian representative data. Our PDD parameters (PDD at 5 cm, 10 cm and 20 cm) were all within 0.5% from Varian data except for those for a field size of 30 × 30 cm<sup>2</sup> (0.6%). They were also within the range for five TrueBeam linacs presented in Gilde-Hurst *et al.*'s study [5] except for those for a field size of 30 × 30 cm<sup>2</sup>.  $d_{\max}$  (1.36 cm) for our energy was within the Varian TrueBeam STx specifications (1.50 ± 0.15 cm). Our profile parameter (lateral distance between 20% and 80% isodose curves at a depth of 10 cm) and Varian representative data had also good agreement within 0.7 mm. For a field size of 3 × 3 cm<sup>2</sup>, profiles had much smaller lateral distances (3.0 mm for cross-plane and 3.6 mm for in-plane) than

Varian representative data (5.4 mm) because our profiles were measured using a diode detector and Varian representative data were generated using an ion chamber (CC13, IBA Dosimetry, Schwarzenbruck, Germany). Comparing our profiles measured using an ion chamber (Sun Nuclear SNC125c™) with Varian representative data, the difference becomes smaller ( $\leq 0.5$  mm). Our PDD and profile parameters for stereotactic cones were not compared with Varian representative data because their measurement setups were different from ours.

**Table 4** presents OFs for jaw-collimated fields and stereotactic cones. OF decreases with decreasing field size and it drastically decreases for square fields  $< 2 \times 2$  cm<sup>2</sup> and cones  $< 7.5$  mm. This study shows that OFs for jaw-collimated square fields had good agreement with those in the literature (**Table 4**). Shende *et al.* reported OFs for field sizes from  $3 \times 3$  cm<sup>2</sup> to  $40 \times 40$  cm<sup>2</sup> measured using an ion chamber [19]. The OF differences between their study and our study are within  $\pm 0.53\%$ . Masanga *et al.* reported OFs for field sizes from  $0.6 \times 0.6$  cm<sup>2</sup> to  $4 \times 4$  cm<sup>2</sup> measured using the Edge detector [20]. The OF differences from our study are within  $\pm 0.55\%$  except for a field size of  $1 \times 1$  cm<sup>2</sup> ( $-1.22\%$  difference). Both studies measured OFs at a depth of 10 cm and SSD of 90 cm, whereas our study measured OFs at a depth of 10 cm and SSD of 100 cm. The Monte Carlo simulation (0.717 for  $1 \times 1$  cm<sup>2</sup> and 0.807 for  $2 \times 2$  cm<sup>2</sup>) performed by Feng *et al.* supports our study (0.11% and 0.55% differences, respectively) [21]. Their setup (depth of 10 cm and SSD of 100 cm) was the same as our study. To our knowledge, there are no published data for the same measurement setup (depth of 10 cm; SSD of 100 cm; normalized to a field size of  $10 \times 10$  cm<sup>2</sup>) for comparison. Varian representative data for cones were obtained at a depth of 5 cm and hence, they were not compared with our OFs.

**Table 4.** Measured output factors for jaw-collimated square fields and stereotactic cones. The output factors were defined at a depth of 10 cm and SSD of 100 cm and were normalized to a field size of  $10 \times 10$  cm<sup>2</sup>.

Field size (cm <sup>2</sup> )	This study	Shende <i>et al.</i> [19]*	Masanga <i>et al.</i> [20]*	Cone diameter (mm)	This study
$0.6 \times 0.6$	0.5722	Not available	0.5690	4	0.5018
$1 \times 1$	0.7162	Not available	0.7250	5	0.5705
$2 \times 2$	0.8114	Not available	0.8070	7.5	0.6671
$3 \times 3$	0.8434	0.8474	0.8440	10	0.7186
$4 \times 4$	0.8766	0.8799	0.8800	12.5	0.7534
$5 \times 5$	0.9062	0.9068	Not available	15	0.7799
$6 \times 6$	0.9310	0.9314	Not available	17.5	0.7971
$8 \times 8$	0.9708	0.9699	Not available		
$10 \times 10$	1.0000	1.0000	1.0000		
$15 \times 15$	1.0495	1.0496	Not available		
$20 \times 20$	1.0805	1.0829	Not available		
$30 \times 30$	1.1142	1.1184	Not available		
$40 \times 40$	1.1252	1.1312	Not available		

\*Output factors were measured at a depth of 10 cm and SSD of 90 cm.

Two factors need to be considered when OFs for small jaw-collimated fields are measured and the factors would depend on the detector selection. The first factor is the daisy-chain method. Diode detectors exhibit energy dependent response due to low energy scattered photons, resulting in a non-linear increase of the response with increasing field size [13]. For this reason, output factors directly normalized to a relatively large field size of  $10 \times 10 \text{ cm}^2$  would be inaccurate for small fields. The daisy-chain method mitigates this effect by normalizing to an intermediate field size (e.g.,  $4 \times 4 \text{ cm}^2$ ) using two different detectors (a diode and an ion chamber). Sharma *et al.* reported up to  $-5\%$  variation of OFs for the Edge detector when OFs measured using the daisy-chain method were compared with OFs directly normalized to a field size of  $10 \times 10 \text{ cm}^2$  for cones [22]. In our study, the OF difference between with and without the daisy-chain method for cones was less than 1% and OFs were underestimated without the daisy-chain method. The second factor is a field output correction factor. The Edge detector used in this study is known to be good for field sizes from  $0.5 \times 0.5 \text{ cm}^2$  to  $10 \times 10 \text{ cm}^2$  but it over-responds for small fields because of the extra perturbation by the increased electron fluence and higher stopping power in silicon [23] and large differences ( $>2\%$ ) between Edge and other detectors become noticeable for a field size  $< 2 \times 2 \text{ cm}^2$  [13] [14]. To take into account its over-response, therefore, for field sizes  $< 2 \times 2 \text{ cm}^2$ , field output correction factors need to be multiplied by measured OFs.

#### ***MLC model parameters and OFs for MLC-collimated square fields***

**Figure 8** shows measured profiles for MLC-collimated fields in comparison with calculated profiles in RayStation. The optimal values for MLC x-position offset, gain and curvature were  $0.006 \text{ cm}$ ,  $0.000 \text{ cm}^{-1}$  and  $0.000 \text{ cm}^{-2}$ , respectively. The optimal value for MLC y-position gain was  $-0.008 \text{ cm}^{-1}$ . **Figure 9(a)** and **Figure 9(b)** show measured versus calculated profiles for leaf tip width and tongue and groove width, respectively. When comparing calculated profiles with leaf tip widths of  $0.2 \text{ cm}$ ,  $0.25 \text{ cm}$  and  $0.3 \text{ cm}$  with the measured one, the optimal value was found to be  $0.25 \text{ cm}$ . Similarly, among calculated profiles with tongue and groove widths of  $0.03 \text{ cm}$ ,  $0.04 \text{ cm}$  and  $0.05 \text{ cm}$ , the profile with a tongue and groove width of  $0.04 \text{ cm}$  matched best the measured one. In **Figure 9(b)**, two inner tongue and groove areas for  $2.5 \text{ mm}$  leaves are shown. Measured MLC transmission was  $0.91\%$ . **Table 5** lists MLC parameter values found in this study.

In this study, optimal values for MLC parameters were determined from direct measurements. PDDs and OFs for MLC-collimated fields are required when profiles are imported in RayStation but they do not directly affect the determination of MLC offset, gain and curvature values. These three parameters have a relationship with MLC leaf end position ( $x_{\text{end}}$ ) and MLC leaf tip position ( $x_{\text{tip}}$ ):  $x_{\text{tip}} = x_{\text{end}} + \text{offset} + \text{gain} \cdot x_{\text{end}} + \text{curvature} \cdot x_{\text{end}}^2$  [7]. In our study, the parameters were determined from the best match between measured profiles and calculated profiles for MLC-collimated fields. Another way to determine these values is to fit a 2<sup>nd</sup> order polynomial to geometric offset ( $=x_{\text{tip}} - x_{\text{end}}$ ) values as a function of MLC leaf end position ( $x_{\text{end}}$ ) [7]. In RayStation, the rounded leaf end is modeled

as a region with one-half the thickness of the MLC leaf which has a transmission of  $\sqrt{T}$  where  $T$  is the intraleaf leakage [7] [24]. The leaf tip width is defined as the width of the MLC region, whereas the leaf tip offset is defined as the MLC offset from the nominal position [24]. These two parameters (leaf tip width and leaf tip offset) determine the radiation edge and penumbra of MLC-collimated fields and affect OFs for MLC-collimated fields [7] [24]. The tongue and groove area is also modeled as a region with one-half the thickness of the leaf and tongue and groove width [7]. While Chen *et al.* iteratively derived MLC parameters from IMRT/VMAT QA results [7], this study determined leaf tip width and tongue and groove width from measurements using custom plans (Figure 3 and Figure 4). The MLC leaf radiation transmission is modeled using an average transmission factor of MLC interleaf and intraleaf leakage [7]. The MLC transmission (0.91%) measured in this study was in agreement with the finding (0.9%) of Kim *et al.* for the same MLC type (Varian HD120™ MLC) and the same energy (6 MV FFF) [25].

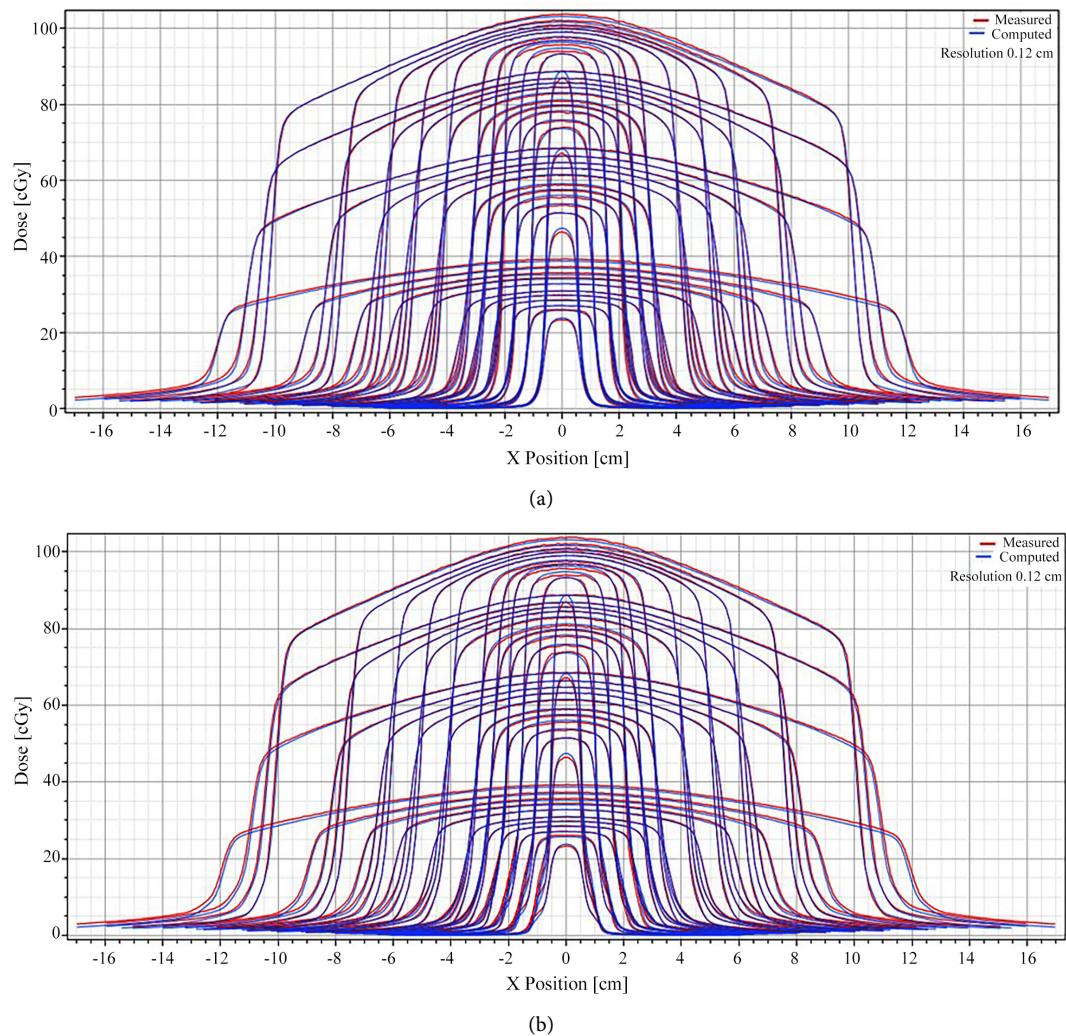


**Figure 8.** (a) Cross-plane and (b) in-plane profiles for MLC-collimated square fields from  $1 \times 1 \text{ cm}^2$  to  $20 \times 20 \text{ cm}^2$ .

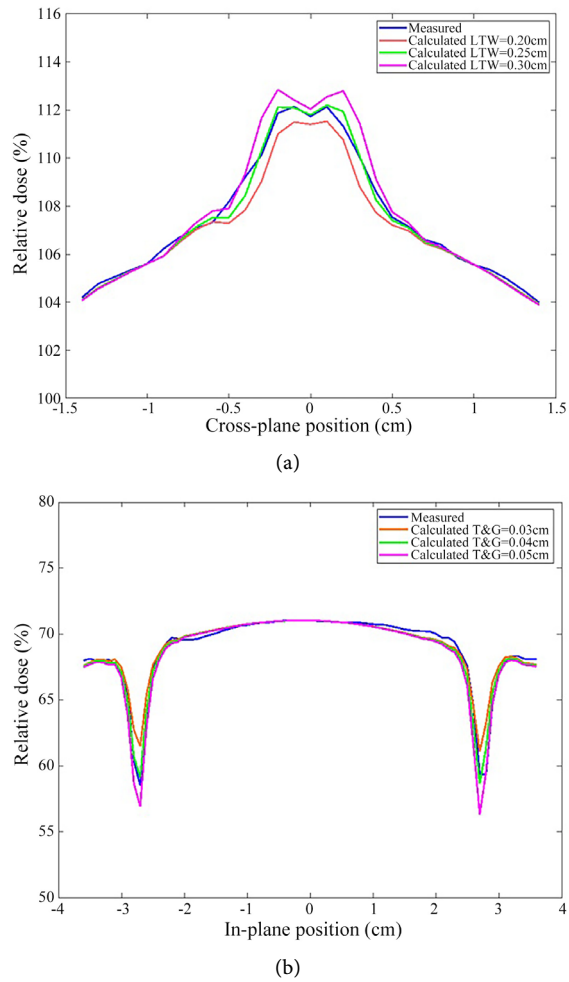


**Figure 9.** (a) Measured profile in comparison with calculated profiles with leaf tip widths of 0.2 cm, 0.25 cm and 0.3 cm and (b) measured profile in comparison with calculated profiles with tongue and groove widths of 0.03 cm, 0.04 cm and 0.05 cm.

**Table 5.** Results for MLC parameters and other measurements.

MLC Parameters	Value
X-position offset	0.006 cm
X-position gain	0.000 cm <sup>-1</sup>
X-position curvature	0.000 cm <sup>-2</sup>
Y-position gain	-0.008 cm <sup>-1</sup>
Leaf tip width	0.25 cm
Tongue and groove	0.04 cm
MLC transmission	0.91%
Others	Value
d <sub>max</sub>	1.36 cm
X-jaws transmission	0.36%
Dose output*	0.632 cGy/MU
P <sub>pol</sub>	1.0006
P <sub>ion</sub>	1.0058

\*Dose output was measured for a field size of 10 × 10 cm<sup>2</sup> at a depth of 10 cm and SSD of 100 cm.

**Table 6** presents measured and calculated OFs for MLC-collimated fields. OF decreases with decreasing field size. The differences (%) between measured and calculated OFs are within  $\pm 0.6\%$  except for a field size of  $1 \times 1 \text{ cm}^2$  (1.13%). The largest difference (1.13%) might be attributed to the use of the field output correction factors for jaw-collimated fields. Our result is better than that (2.1% for a field size of  $2 \times 2 \text{ cm}^2$  for 6 MV) reported in Chen *et al.* [7]. The comparison between measurements and calculations verifies that MLC leaf tip offset and leaf tip width values were relatively well determined. OFs for jaw-collimated fields had good agreement ( $\leq \pm 0.38\%$ ) with OFs for MLC-collimated fields except for that (2.53%) for a field size of  $1 \times 1 \text{ cm}^2$  (**Table 4** and **Table 6**). This might be attributed to more scatter with the MLC-collimated field. The MLC position is defined as the MLC leaf end position [7] and therefore, the rounded edge of the MLC is in the beam. When the jaw position is the same as MLC position, more scatter from the rounded edge will be collected at the center of the field. This effect would be more pronounced for small fields such as  $1 \times 1 \text{ cm}^2$ . In this study, the difference increases with decreasing field size for fields sizes  $\leq 6 \times 6 \text{ cm}^2$  (**Table 4** and **Table 6**).

#### ***Absolute dose calibration***

Dose output at the absolute dose calibration point (depth of 10 cm) was 0.632 cGy/MU.  $P_{\text{pol}}$  and  $P_{\text{ion}}$  measured during dose calibration were 1.0006 and 1.0058, respectively. **Table 5** lists these values. Our absolute dose calibration had good agreement with that reported in the literature. Dose output at a depth of 10 cm (0.632 cGy/MU) was within the value ( $0.633 \pm 0.01$ ) reported in Glide-Hurst *et al.* [5]. While  $P_{\text{ion}}$  (1.0058) was also within the value ( $1.006 \pm 0.02$ ) reported in Glide-Hurst *et al.*,  $P_{\text{pol}}$  (1.0006) was slightly off (0.06%) from the literature ( $0.999 \pm 0.001$ ) [5]. The difference between  $\%dd(10)_x$  (*i.e.*,  $\%dd(10, 9.5)$ , AAPM TG-51 approach) and  $\%dd(10, 10)$  (TRS 483 approach) was 0.65%, resulting in only 0.02% difference in  $k_Q$ . After considering  $\%dd(10, 10)$  of TRS 483, the  $k_Q$  difference between AAPM TG 51 and addendum to AAPM TG 51 was 0.23%. As a result, the output difference between AAPM TG 51 without TRS 483 approach and addendum to AAPM TG 51 with TRS 483 approach was 0.25% ( $=0.02\% + 0.23\%$ ).

### **3.2. Beam Model/MLC Model Validation**

Results for MPPG 5.a. Tests 7.3, 7.4 and 7.5 are shown in **Table 7**. Four plans (Multitarget, Mock prostate, CShape (easier) and CShape (harder)) in the AAPM TG-119 report had gamma passing rates of  $\geq 98.0\%$  and  $\geq 96.0\%$  with 3%/3 mm and 2%/2 mm, respectively. The Mock head and neck plan had lower passing rates of 97.0% and 88.2% with 3%/3 mm and 2%/2 mm, respectively. Clinical SRS DCAT plans had mean passing rates of 99.7% (2%/1 mm) and 99.3% (1%/1 mm). SRS VMAT plans had lower mean passing rates of 96.1% (2%/1 mm) and 92.2% (1%/1 mm). Clinical SBRT DCAT plans had similar trends: DCAT plans (100% (2%/1 mm) and 96.8% (1%/1 mm)) had higher mean passing rates than VMAT plans (98.2% (2%/1 mm) and 94.8% (1%/1 mm)). End-to-end testing results showed 0.20% and 0.53% differences between mea-

measurements and calculations for the SRS VMAT plan and SRS CCAT plan, respectively.

The MPPG 5.a. Test 7.3 and Test 7.4 results show that our beam model and MLC model are acceptable. Gamma passing rates of AAPM TG-119 plans performed in this study were higher than those (Table XI) reported in the AAPM TG 119 [18]. In the TG-119 report, the measurements were made using film and film measurement uncertainties could have caused lower passing rates. The results (100% for all the plans) reported in Chen *et al.* [7] are better than our results. Our TG-119 plans were highly modulated and all the failing points occurred in low dose regions. Our clinical SRS and SBRT plan QA results showed very high passing rates even with criteria of 2%/1 mm and 1%/1 mm. Although the MLC parameter values found in this study were determined while MLCs were not moving, validation test results are fairly comparable to other studies [7] [26].

**Table 6.** Measured and calculated output factors for MLC-collimated square fields. The output factors were defined at a depth of 10 cm and SSD of 100 cm and were normalized to a field size of 10 × 10 cm<sup>2</sup>.

Field size (cm <sup>2</sup> )	Measured	Calculated	Measured/Calculated (% diff.)
1 × 1	0.73429	0.74265	0.98874 (1.13%)
2 × 2	0.81429	0.81158	1.00333 (0.33%)
3 × 3	0.84574	0.84629	0.99935 (0.07%)
4 × 4	0.87839	0.88337	0.99436 (0.56%)
5 × 5	0.90707	0.91007	0.99670 (0.33%)
6 × 6	0.93103	0.93352	0.99733 (0.27%)
8 × 8	0.97033	0.97282	0.99744 (0.26%)
10 × 10	1.00000	1.00000	1.00000 (0.00%)
12 × 12	1.02331	1.02337	0.99994 (0.01%)
15 × 15	1.05128	1.04968	1.00153 (0.15%)
20 × 20	1.08454	1.08137	1.00293 (0.29%)

**Table 7.** MPPG 5.a. Test results. For Tests 7.3 and 7.4, absolute dose mode, global normalization and a threshold of 10% were used.

<b>MPPG 5.a. Test 7.3 (AAPM TG-119 tests): Gamma passing rate</b>									
Multitarget		Mock prostate		Mock head and neck		CShape (easier)		CShape (harder)	
3%/3	2%/2	3%/3 mm	2%/2 mm	3%/3 mm	2%/2 mm	3%/3 mm	2%/2 mm	3%/3 mm	2%/2 mm
99.4%	97.3%	99.7%	98.9%	97.0%	88.2%	99.7%	98.7%	98.3%	96.3%
<b>MPPG 5.a. Test 7.4 (clinical tests): Gamma passing rate</b>									
SRS (DCAT†)		SRS (VMAT‡)		SBRT (DCAT)		SBRT (VMAT)			
2%/1 mm	1%/1 mm	2%/1 mm	1%/1 mm	2%/1 mm	1%/1 mm	2%/1 mm	1%/1 mm		
99.7%	99.3%	96.1%	92.2%	100%	96.8%	98.2%	94.8%		
<b>MPPG 5.a. Test 7.5 (end-to-end testing): Ion chamber measurement result</b>									
SRS (VMAT)					SRS (CCAT* with a 17.5 mm cone)				
0.20%					0.53%				

†Dynamic conformal arc therapy; ‡Volumetric modulated arc therapy; \*Circular collimator arc therapy.

Our end-to-end testing results (MPPG 5.a. Test 7.5) also support acceptable beam and MLC models. The plans for end-to-end testing had a field size ( $\sim 1.9 \times 1.9 \text{ cm}^2$ ) and a cone diameter (17.5 mm, equivalent square field of 15.5 mm) large enough compared with the size of the ion chamber. Although the MLC-based SRS plan used VMAT, the plan was not highly modulated and MLCs were mostly open with gantry rotation. The TRS 483 reported that field output correction factors for the Exradin A16 ion chamber are 1.003 and 1.008 for  $2 \times 2 \text{ cm}^2$  and  $1.5 \times 1.5 \text{ cm}^2$ , respectively [13], implying that the ion chamber would underestimate dose by 0.3% and 0.8% for the small fields. Considering these factors, our end-to-end testing results seem acceptable.

#### 4. Conclusion

In this study, following the comprehensive steps described in detail, dosimetric data required by RayStation were acquired for the TrueBeam STx 6 MV FFF beam. For beam modeling, PDDs, profiles and output factors for jaw-collimated fields and stereotactic cones and X-jaws transmission were measured. For MLC modeling, MLC model parameters (offset, gain, curvature, leaf tip width, tongue and groove and transmission) and output factors for MLC-collimated fields were measured. Absolute dose calibration was also performed. The dosimetric data acquired in this study had good agreement with those in the literature. For beam model and MLC model validation, MPPG 5.a. tests were performed. The results for MPPG 5.a. Test 7.3 (AAPM TG 119 tests), Test 7.4 (clinical tests) and Test 7.5 (complete end-to-end test) showed that our beam model and MLC model are well acceptable for SRS and SBRT treatments. Since there is a paucity of the existing information on detailed commissioning steps and comprehensive dosimetric data for the RayStation TPS in the literature, this study will be a useful and practical reference for other clinics or institutions which will embark on commissioning the TrueBeam STx 6 MV FFF beam in the RayStation TPS.

#### Acknowledgements

The authors would like to thank Ms. Carmen Sawyers and Mr. Sam Painter from RaySearch Laboratories for their help with beam modeling and MLC modeling. The authors would also like to thank Mr. Alessandro Savini for sharing his work on MLC model parameter measurements.

#### Conflicts of Interest

The authors declare no conflicts of interest regarding the publication of this paper.

#### References

- [1] Fogliata, A., Fleckenstein, J., Schneider, F., Pachoud, M., Ghandour, S., Krauss, H., *et al.* (2016) Flattening Filter Free Beams from TrueBeam and Versa HD Units: Evaluation of the Parameters for Quality Assurance. *Medical Physics*, **43**, 205. <https://doi.org/10.1118/1.4938060>

- [2] Chang, Z., Wu, Q., Adamson, J., Ren, L., Bowsher, J., Yan, H., *et al.* (2012) Commissioning and Dosimetric Characteristics of TrueBeam System: Composite Data of Three Truebeam Machines. *Medical Physics*, **39**, 6981-7018. <https://doi.org/10.1118/1.4762682>
- [3] Narayanasamy, G., Saenz, D., Cruz, W., Ha, C.S., Papanikolaou, N. and Stathakis, S. (2016) Commissioning an Elekta Versa HD Linear Accelerator. *Journal of Applied Clinical Medical Physics*, **17**, 179-191. <https://doi.org/10.1120/jacmp.v17i1.5799>
- [4] Thomas, E.M., Popple, R.A., Prendergast, B.M., Clark, G.M., Dobelbower, M.C. and Fiveash, J.B. (2013) Effects of Flattening Filter-Free and Volumetric-Modulated Arc Therapy Delivery on Treatment Efficiency. *Journal of Applied Clinical Medical Physics*, **14**, 155-166. <https://doi.org/10.1120/jacmp.v14i6.4328>
- [5] Glide-Hurst, C., Bellon, M., Foster, R., Altunbas, C., Speiser, M., Altman, M., *et al.* (2013) Commissioning of the Varian TrueBeam Linear Accelerator: A Multi-Institutional Study. *Medical Physics*, **40**, Article ID: 031719. <https://doi.org/10.1118/1.4790563>
- [6] Beyer, G.P. (2013) Commissioning Measurements for Photon Beam Data on Three TrueBeam Linear Accelerators, and Comparison with Trilogy and Clinac 2100 Linear Accelerators. *Journal of Applied Clinical Medical Physics*, **14**, 273-288. <https://doi.org/10.1120/jacmp.v14i1.4077>
- [7] Chen, S., Yi, B.Y., Yang, X., Xu, H., Prado, K.L. and D'Souza WD. (2015) Optimizing the MLC Model Parameters for IMRT in the RayStation Treatment Planning System. *Journal of Applied Clinical Medical Physics*, **16**, 322-332. <https://doi.org/10.1120/jacmp.v16i5.5548>
- [8] Savini, A., Bartolucci, F., Fidanza, C., Rosica, F. and Orlandi, G. (2016) Optimisation and Assessment of the MLC Model in the Raystation Treatment Planning System. *Radiotherapy and Oncology*, **119**, S380-S381. [https://doi.org/10.1016/S0167-8140\(16\)32056-4](https://doi.org/10.1016/S0167-8140(16)32056-4)
- [9] Saez, J., Hernandez, V., Goossens, J., Kerf, G.D. and Verellen, D. (2020) A Novel Procedure for Determining the Optimal MLC Configuration Parameters in Treatment Planning Systems Based on Measurements with a Farmer Chamber. *Physics in Medicine & Biology*, **65**, Article ID: 155006. <https://doi.org/10.1088/1361-6560/ab8cd5>
- [10] Das, I.J., Cheng, C.W., Watts, R.J., Ahnesjö, A., Gibbons, J., Li, X.A., *et al.* (2009) Accelerator Beam Data Commissioning Equipment and Procedures: Report of the TG-106 of the Therapy Physics Committee of the AAPM. *Medical Physics*, **35**, 4186-4215. <https://doi.org/10.1118/1.2969070>
- [11] Li, J., Lu, B., Yan, G., Huang, Y. and Liu, C. (2012) SU-D-BRCD-02: A Novel Cylindrical 3D Water Scanner for Beam Data Collection: I. Validation of the Automatic-Setup. *Medical Physics*, **39**, 3613-3613. <https://doi.org/10.1118/1.4734668>
- [12] Pönisch, F., Titt, U., Vassiliev, O.N., Kry, S.F. and Mohan, R. (2006) Properties of Unflattened Photon Beams Shaped by a Multileaf Collimator. *Medical Physics*, **33**, 1738-1746. <https://doi.org/10.1118/1.2201149>
- [13] IAEA and AAPM. (2017) Dosimetry of Small Static Fields Used in External Beam Radiotherapy. Technical Reports Series No. 483. International Atomic Energy Agency, Vienna. <https://www.iaea.org/publications/11075/dosimetry-of-small-static-fields-used-in-external-beam-radiotherapy>.
- [14] Tanny, S., Sperling, N. and Parsai, E.I. (2015) Correction Factor Measurements for Multiple Detectors Used in Small Field Dosimetry on the Varian Edge Radiosurgery System. *Medical Physics*, **42**, 5370-5376. <https://doi.org/10.1118/1.4928602>

- [15] Smilowitz, J.B., Das, I.J., Feygelman, V., Fraass, B.A., Kry, S.F., Marshall, I.R., Mihailidis, D.N., *et al.* (2015) AAPM Medical Physics Practice Guideline 5.a.: Commissioning and QA of Treatment Planning Dose Calculations—Megavoltage Photon and Electron Beams. *Journal of Applied Clinical Medical Physics*, **16**, 14-34. <https://doi.org/10.1120/jacmp.v16i5.5768>
- [16] Almond, P.R., Biggs, P.J., Coursey, B.M., Hanson, W.F., Huq, M.S., Nath, R., *et al.* (1999) AAPM's TG-51 Protocol for Clinical Reference Dosimetry of High-Energy Photon and Electron Beams. *Medical Physics*, **26**, 1847-1870. <https://doi.org/10.1118/1.598691>
- [17] McEwen, M., DeWerd, L., Ibbott, G., Followill, D., Rogers, D.W.O., Seltzer, S., *et al.* (2014) Addendum to the AAPM's TG-51 Protocol for Clinical Reference Dosimetry of High-Energy Photon Beams. *Medical Physics*, **41**, Article ID: 041501. <https://doi.org/10.1118/1.4866223>
- [18] Ezzell, G.A., Burmeister, J.W., Dogan, N., LoSasso, T.J., Mechalakos, J.G., Mihailidis, D., *et al.* (2009) IMRT Commissioning: Multiple Institution Planning and Dosimetry Comparisons, a Report from AAPM Task Group 119. *Medical Physics*, **36**, 5359-5373. <https://doi.org/10.1118/1.3238104>
- [19] Shende, R., Gupta, G., Patel, G. and Kumar, S. (2016) Commissioning of TrueBeam™ Medical Linear Accelerator: Quantitative and Qualitative Dosimetric Analysis and Comparison of Flattening Filter (FF) and Flattening Filter Free (FFF) Beam. *International Journal of Medical Physics, Clinical Engineering and Radiation Oncology*, **5**, 51-69. <http://dx.doi.org/10.4236/ijmpcero.2016.51006>
- [20] Masanga, W., Tangboonduangjit, P., Khamfongkhrua, C. and Tannanonta, C. (2016) Determination of Small Field Output Factors in 6 and 10 MV Flattening Filter Free Photon Beams Using Various Detectors. *Journal of Physics Conference Series*, **694**, Article ID: 012027. <https://doi.org/10.1088/1742-6596/694/1/012027>
- [21] Feng, Z., Yue, H., Zhang, Y., Wu, H., Cheng, J. and Su, X. (2016) Monte Carlo Simulation of Beam Characteristics from Small Fields Based on TrueBeam Flattening-Filter-Free Mode. *Radiation Oncology*, **11**, Article No. 30. <https://doi.org/10.1186/s13014-016-0601-2>
- [22] Sharma, D.S., Chaudhary, R.K., Sharma, S.D., Pilakkal, S., Rasal, S.K., Sawant, M.B., *et al.* (2017) Experimental Determination of Stereotactic Cone Size and Detector Specific Output Correction Factor. *The British Journal of Radiology*, **90**, Article ID: 20160918. <https://doi.org/10.1259/bjr.20160918>
- [23] Qin, Y.J., Zhong, H.L., Wen, N., Snyder, K., Huang, Y.M. and Chetty, I.J. (2016) Deriving Detector-Specific Correction Factors for Rectangular Small Fields Using a Scintillator Detector. *Journal of Applied Clinical Medical Physics*, **17**, 379-391. <https://doi.org/10.1120/jacmp.v17i6.6433>
- [24] Koger, B., Price, R., Wang, D., Toomeh, D., Geneser, S. and Ford, E. (2020) Impact of the MLC Leaf-Tip Model in a Commercial TPS: Dose Calculation Limitations and IROC-H Phantom Failures. *Journal of Applied Clinical Medical Physics*, **21**, 82-88. <https://doi.org/10.1002/acm2.12819>
- [25] Kim, J., Han, J.S., Hsia, A.T., Li, S., Xu, Z. and Ryu, S. (2018) Relationship between Dosimetric Leaf Gap and Dose Calculation Errors for High Definition Multi-Leaf Collimators in Radiotherapy. *Physics and Imaging in Radiation Oncology*, **5**, 31-36. <https://doi.org/10.1016/j.phro.2018.01.003>
- [26] Mzenda, B., Mugabe, K.V., Sims, R., Godwin, G. and Loria, D. (2014) Modeling and Dosimetric Performance Evaluation of the RayStation Treatment Planning System. *Journal of Applied Clinical Medical Physics*, **15**, 29-46. <https://doi.org/10.1120/jacmp.v15i5.4787>